

The unexpected magnetism in 2D group-IV-doped GaN for spintronic applications

Rui Zhao, Rui Guo, Yiran Peng, Yanfeng Ge, Yong Liu, and Wenhui Wan*

State Key Laboratory of Metastable Materials Science and Technology & Key Laboratory for Microstructural Material Physics of Hebei Province, School of Science, Yanshan University, Qinhuangdao, 066004, P. R. China

E-mail: wwh@ysu.edu.cn

December 2022

Abstract. In this study, we systematically investigated the structural and magnetic properties of group-IV-doped monolayer GaN by first-principles calculations. Among the group-IV element, only Ge and Sn atoms with large atomic radii can form a buckling substituted doping structure with an in-plane magnetic moment of $1 \mu_B$ per dopant. The compressive strains enhance the in-plane magnetic anisotropy, while tensile strains tend to destroy the magnetic moment of dopants. Both Ge and Sn atoms can stay on the same side of monolayer GaN to form anti-ferromagnetic semiconductors due to the large diffusion barrier for crossing to the monolayer GaN. The intrinsic Ga or N vacancies will eliminate the magnetic moments of group-IV dopants due to the charge transferring from the dopants to intrinsic vacancies. The N-rich growth conditions and a plentiful supply of Ge or Sn dopants to fill the intrinsic vacancies help to maintain the magnetic properties of group-IV-doped monolayer GaN.

1. Introduction

It is long sought to combine magnetic and semiconducting properties within a single material for the applications of spintronics. Transitional dilute magnetic semiconductors (DMSs) were achieved by doping group III-V and II-VI semiconductors with transition metal (TM) ions, whose partially filled d or f orbitals contribute to the magnetic moment [1, 2]. Besides that, bulk oxides of nonmagnetic (NM) cations such as ZnO and SnO₂ can also exhibit room-temperature ferromagnetism, namely “ d^0 ferromagnetism”. The origin of d^0 magnetism was explained by native lattice defect sites [4, 5] or spin-split defect impurity bands of surface defects [6]. In 2017, 2D stable magnetism were demonstrated in atomically thin CrI₃ [7] and Cr₂Ge₂Te₆ [8]. Based on that, the search for d^0 magnetism in 2D materials also becomes a fast-growing field and attracts much research interest.

Until now, d^0 magnetism has been predicted in partially hydrogenated silicene [9], monolayer MoS₂ [10], monolayer AlN [11, 12, 13], and monolayer SnS₂ [14] doped with NM elements. Gallium Nitride (GaN) is a wide-band-gap semiconductor (~ 3.4 eV)

with a hard and hexagonal crystal structure [15]. GaN has been widely applied in light-emitting diodes, laser diodes, semiconductor power devices, high-frequency devices, and water-splitting devices [16, 17]. Compared to many TM ions which can form DMSs in doped bulk GaN [1, 2, 18], group-IV elements exhibit as non-magnetic (NM) n-type dopants in bulk GaN [19, 20]. Recently, two-dimensional (2D) GaN has been synthesized with graphene as a capping sheet utilizing migration-enhanced encapsulation growth [21, 22]. 2D pristine GaN is an NM semiconductor with an indirect band gap, which prevents its application in spintronics. The doping of TM ions can induce magnetism in 2D GaN [23, 24, 25]. Therefore, it is straight and significant to explore the existence of the d^0 magnetism in 2D GaN for spintronics applications.

In the case of intrinsic defects, Ga vacancies can induce room-temperature ferromagnetism in GaN films, which has been observed in the experiment [26]. Each Ga vacancy induces a magnetic moment of $3 \mu_B$ in monolayer GaN, which can be further tuned with the doping concentration of Mg or Si atoms [27, 28]. N vacancies have smaller formation energy than that of Ga vacancies in both bulk and monolayer GaN [29, 28]. There is a contradiction in the magnetic state of N vacancy. González et al. predicted that each N vacancy exhibited a magnetic moment of $1 \mu_B$ [30], while Gao et al. predicted that N vacancy was NM and could not introduce magnetism into monolayer GaN [31]. In the case of external doping, in 2015, Mu predicted that the adsorption of F or N adatoms at low coverage made monolayer GaN become a magnetic half-metal with a high Curie temperature [32]. The $2p$ orbitals of N atoms make the main contribution to the magnetic moment in F- or N-absorbed monolayer GaN [32]. In 2018, it was found that adatoms including B, C, N, Al, Si, Ga, Ge, As atoms, and O_2 molecular preferred to be located at top of the N atom of monolayer GaN [33, 34]. These adatoms induce localized impurity states in the fundamental band gap of monolayer GaN, thereby bringing in the non-zero magnetic moment [33, 34]. However, Kadioglu et al. further found that the aforementioned dopants were more likely to be substituted defects, as the corresponding formation energy is lower than that of adatoms' configurations [34]. Unfortunately, among all the substituted defects of the aforementioned dopants, only N substitution of Ga and C substitution of N can form d^0 magnetism in monolayer GaN, while others are NM [34]. Here, we focus on the group-IV element including C, Si, Ge, and Sn. It was previously believed that group-IV atoms tend to substitute the Ga atoms rather than N atoms in monolayer GaN, serving as NM n-type dopants [34, 35, 36]. We noticed that in previous works the substituted group-IV atoms were directly located at the origin position of the Ga atom in monolayer GaN [34, 35]. These group-IV atoms in the GaN plane can effectively hybridize with the neighboring N atoms and exhibit zero magnetic moment. However, in 2014, Gupta et al. predicted that the substituted Si atoms in monolayer BN tend to leave the BN plane and form a bucking structure [37], due to the larger atomic radius of the Si atom than the B atom. This kind of bucking structure weakens the hybridization between the Si atom and the neighboring N atoms, making the Si atom own an unpaired electron that produces a magnetic moment of $1 \mu_B$ [37]. Since the geometry of the doping configuration is crucial to control the magnetic

properties of 2D materials, monolayer GaN with the substituted group-IV dopants in the bucking doping configuration calls for a timely investigation. The relative works have not been reported so far.

In this work, the preferential occupancy site, magnetic configuration, electronic structure, and diffusion barrier of group-IV atoms in monolayer GaN at a low doping concentration were investigated by the first-principles calculations. We found that Ge and Sn atoms preferred to form a buckling substituted structure and exhibited a magnetic moment of $1 \mu_B$ per dopant atom in monolayer GaN. Biaxial strain can regulate magnetic anisotropy energy (MAE) and magnetic moment of dopants. We investigated the magnetic coupling between the dopant atoms which is located at the different or same side of GaN plane. At last, the effect of intrinsic vacancies on the magnetic properties of group-IV-doped monolayer GaN was analyzed.

2. Computational details

All the first-principles calculations were performed by the Vienna ab initio simulation package (VASP) [38] with the projector augmented wave (PAW) [39] pseudopotentials and Perdew–Burke–Ernzerhof (PBE) [40] exchange-correlation functionals. A kinetic energy cutoff of 520 eV was adopted. The Brillouin zone integrations were performed with $12 \times 12 \times 1$ Gamma-centered \mathbf{k} -mesh [41] for the primitive cell of monolayer GaN. The vacuum layer vertical to monolayer GaN was set to be 20 Å. The convergence criteria of the total energy and force were set to be 10^{-5} eV and 0.01 eV/Å, respectively.

The formation energy E_f was defined as

$$E_f = E_{\text{GaN}+\text{X}} - E_{\text{GaN}} - \mu_{\text{Ga}}n_{\text{Ga}} - \mu_{\text{N}}n_{\text{N}} - \mu_{\text{X}}n_{\text{X}} \quad (1)$$

where E_{GaN} and $E_{\text{GaN}+\text{X}}$ are the total energy of monolayer GaN and monolayer GaN doped with group-IV atom X (X = C, Si, Ge, and Sn), respectively. n is the negative or positive integer that represents the number of the removed or added atoms in monolayer GaN, respectively. μ_{Ga} , μ_{N} , and μ_{X} are the chemical potentials of the Ga, N, and group-IV atom, respectively. We set the μ_{X} as the energy of each group-IV atom in its substance. We further considered the different growth conditions. In Ga-rich growth conditions, μ_{Ga} is equal to the energy of each Ga atom in the Ga substance, while μ_{n} is calculated by $\mu_{\text{n}} = \mu_{\text{GaN}} - \mu_{\text{Ga}}$ with μ_{GaN} be the energy per formula of monolayer GaN. Similarly, for the N-rich growth conditions, μ_{n} equals the energy per N atom in N_2 molecular, and μ_{Ga} was calculated by $\mu_{\text{Ga}} = \mu_{\text{GaN}} - \mu_{\text{N}}$.

The MAE is defined as $\text{MAE} = E_{//} - E_{\perp}$, where $E_{//}$ and E_{\perp} are the energy with magnetization along the in-plane and out-of-plane directions, respectively. The spin-orbit coupling (SOC) effect was considered to calculate the MAE. The positive and negative MAE indicates that the magnetic moment of the group IV dopant prefers to be out-of-plane and in-plane, respectively.

Table 1. The formation energy E_f (eV) and magnetic moment m (μ_B) of single Ge atom doped monolayer GaN in the nonmagnetic (NM) state and magnetic (M) state.

Position	Ga-rich(NM)	N-rich(NM)	Ga-rich(M)	N-rich(M)	m
Ge _{T,Ga}	3.82	3.82	3.40	3.40	2
Ge _{T,N}	2.51	2.51	2.31	2.31	2
Ge _H	3.65	3.65	3.14	3.14	2
Ge _{N,planar}	3.57	3.67	3.36	3.46	1
Ge _{Ga,planar}	1.38	1.28	1.38	1.28	0
Ge _{N,buckling}	2.19	2.29	2.10	2.20	1
Ge _{Ga,buckling}	1.37	1.27	1.25	1.16	1

3. Results and discussion

3.1. Single Ge atom doping in monolayer GaN

Monolayer GaN adopts a planar and hexagonal lattice [see figure 1(a)]. We calculated the lattice constant of monolayer GaN to be 3.255 Å, which agrees well with previous works [26, 28, 42, 43]. The chemical bond length $d_{\text{Ga-N}}$ is 1.88 Å. We first put a single Ge atom in a $6 \times 6 \times 1$ supercell of monolayer GaN. We considered different adsorption configurations including the Ge atom on top of the Ga site (Ge_{T,Ga}) or the N site (Ge_{T,N}); Ge atom in the middle of the hexagonal ring (Ge_H); Ge atom on the bridge site of Ga-N bond (Ge_B) [see figure 1(a)]. We also examined possible substituted configurations which include the substitution of a Ga atom (Ge_{Ga,planar}) or N atom (Ge_{N,planar}) by a Ge atom which stays in the GaN plane; Ge_{Ga,buckling} and Ge_{N,buckling} represent that the substituted Ge atom was pushed out of the GaN plane by a certain buckling height. Considering the effect of the growth conditions, we calculated the formation energy E_f of the above doping configurations under the Ga-rich and N-rich growth conditions, respectively. Moreover, the Ge atom in the NM state and magnetic state were also considered.

Ge_B site is unstable at both NM and magnetic states, and will be transferred to Ge_{T,N} site during the structural relaxation. The results of E_f were summarized in table 1. Firstly, the Ge atom in adsorbed configurations can introduce a magnetic moment of 2 μ_B per Ge atom, as the corresponding E_f of the magnetic state is smaller than that of the NM state. Meanwhile, the E_f of adsorbed configurations are not affected by growth conditions, as the n_{Ga} and n_{N} are zero in equation 1. Secondly, the E_f of substituted doping configurations are generally smaller than that of adsorbed configurations. Moreover, the Ge atom prefers to substitute the Ga atom rather than the N atom in monolayer GaN. The ground magnetic state of Ge_{Ga,planar} is NM, as the initial magnetic state will transition into the NM state. The above results agree well with previous works [34, 35, 36], indicating the reliability of our calculations. Thirdly, compared to the planar Ge_{Ga,planar} configuration, Ge atom in the buckling substituted doping configuration Ge_{Ga,buckling} has a lower E_f in both NM and magnetic states,

thereby being the most stable doping configuration. This can be directly reflected by the evolution of energy of Ge_{Ga} as the Ge atom gets close to the Ga vacancy gradually, as shown in figure A1(a). Three valence electrons of the Ge atom in $\text{Ge}_{\text{Ga,buckling}}$ structure participate in the chemical bonding with three neighboring N atoms, leaving a localized and unpaired electron on the Ge atom which contributes a magnetic moment of $1 \mu_B$. The E_f of $\text{Ge}_{\text{Ga,buckling}}$ can be further reduced in the N-rich growth conditions, as shown in table 1. Thus, Ge atoms indeed can induce non-zero magnetic moment and magnetic properties in monolayer GaN. However, the doping of the Ge atom into monolayer GaN is an endothermal reaction that needs extra energy to promote the doping process.

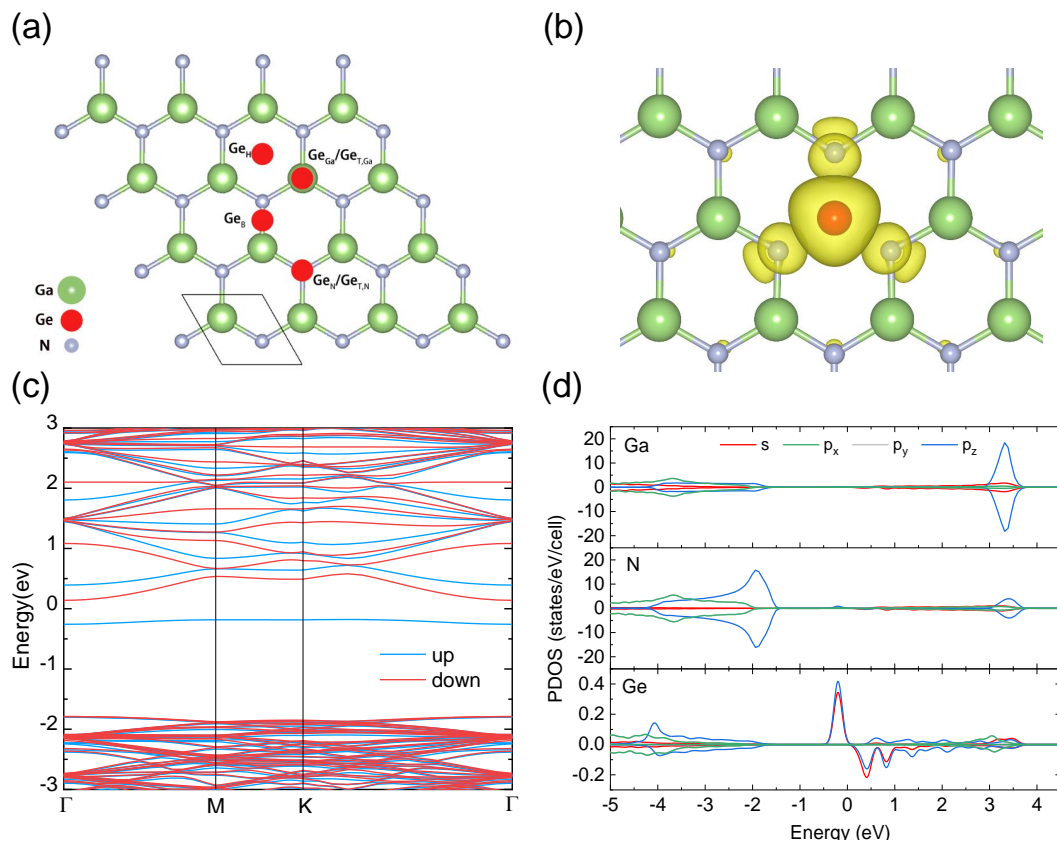


Figure 1. (a) Monolayer GaN with a Ge atom be located at different positions. (b) The spin density of $\text{Ge}_{\text{Ga,buckling}}$ structure. The isosurface is $0.002 \text{ eV}/\text{\AA}^3$. The yellow color represents the positive spin density. The negative spin density is negligible. (c) Energy band and (d) projected density of states of the $\text{Ge}_{\text{Ga,buckling}}$ structure.

We examined the lattice structure and electronic structures of $\text{Ge}_{\text{Ga,buckling}}$ configuration. The buckling height h of Ge dopant is about 0.6 \AA . The optimized Ge-N bond length is 0.01 \AA larger than that of Ga-N bonding. Because the neighboring N atoms get close to the Ge dopant along the in-plane direction, the neighboring Ga-N bond lengths were enlarged by 0.01 \AA . The spin density of $\text{Ge}_{\text{Ga,buckling}}$ is mainly distributed around the Ge atom and its three nearest neighboring N atoms [see figure 1(b)]. Compared to the positive spin density, the negative spin density is negligible.

Figure 1(c) displays the band structure of $\text{Ge}_{\text{Ga,buckling}}$ configuration which still keeps the semiconducting properties. The top valence band and bottom conduction band are comprised of spin-down and spin-up electronic states, respectively. Ge dopant introduces a dispersionless impurity band among the band gap and other impurity bands near the conduction bands of monolayer GaN. Thus, $\text{Ge}_{\text{Ga,buckling}}$ configuration has a band gap of about 0.40 eV at the PBE level [see figure 1(c)]. The s , p_z orbital of the Ge atom and the p_z orbital of the neighboring N atoms around the Ge atom dominate the electronic states around the Fermi level, as shown in the projected density of states (PDOS) in figure 1(d). Through the analysis of the orbital-resolved magnetic moment, we found that the same orbitals dominate the magnetic moment of $\text{Ge}_{\text{Ga,buckling}}$ configuration. On the other side, the contribution of Ga atoms to the magnetic moment can be negligible.

We further compared the energy of $\text{Ge}_{\text{Ga,buckling}}$ configuration with magnetic moment along different directions including [100] [010] [001] [110] [111] directions [see table 3]. The magnetic moment of Ge dopant prefer the in-plane direction. The negative MAE is estimated to be about $-14.55 \mu\text{eV}$ per Ge atom. Moreover, the energy difference of MAE is less than $0.1 \mu\text{eV}$ for magnetic moment lying in the xy -plane. Thus, the MAE of $\text{Ge}_{\text{Ga,buckling}}$ can be seen to be isotropic in the xy -plane.

We also investigated the diffusion of the Ge atom crossing or along the GaN plane. In the vertical direction, there are two symmetry equivalent $\text{Ge}_{\text{Ga,buckling}}$ configuration on both sides of monolayer GaN. The Ge atom can cross the GaN plane and reach the other $\text{Ge}_{\text{Ga,buckling}}$ site. By the nudged elastic band (NEB) method [44], the vertical diffusion barrier ΔE was identified to be the energy difference between the $\text{Ge}_{\text{Ga,buckling}}$ and $\text{Ge}_{\text{Ga,planar}}$, which is about 0.12 eV. On the other side, the diffusion of the Ge atom parallel to the GaN plane can proceed through the low-energy adsorption sites, which is $\text{Ge}_{\text{T,N}} - \text{Ge}_{\text{H}} - \text{Ge}_{\text{T,N}}$ pathway [see figure 2(a)]. Through the NEB method [44], the optimized saddle point was near the Ge_{H} site. The in-plane diffusion barrier ΔE was estimated at 0.82 eV [see figure 2(b)].

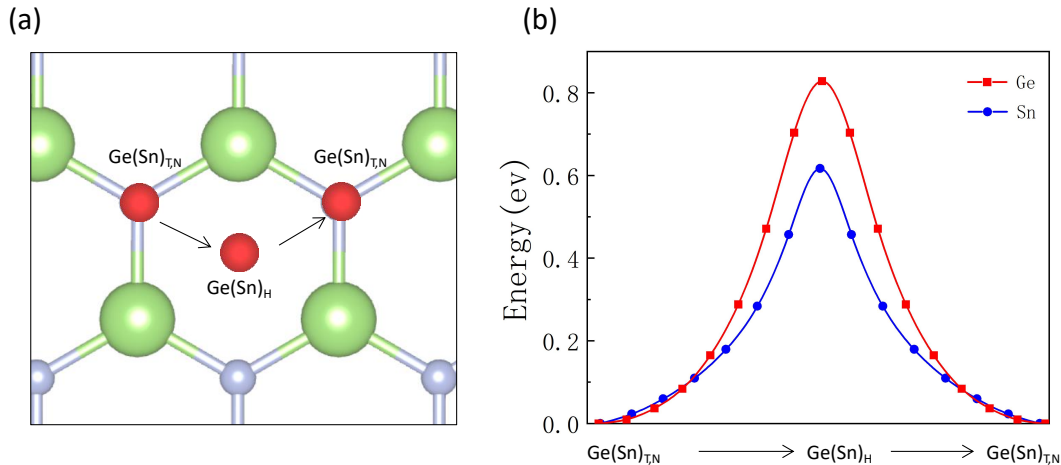


Figure 2. (a) Diffusion path and (b) corresponding energy profile of single Ge and Sn atoms along the surface of monolayer GaN.

Table 2. The formation energy E_f (eV) of single Sn atom doped monolayer GaN in nonmagnetic (NM) state and magnetic (M) state.

Position	Ga-rich(NM)	N-rich(NM)	Ga-rich(M)	N-rich(M)
Sn _{T,Ga}	3.30	3.30	2.91	2.91
Sn _{T,N}	2.58	2.58	2.06	2.06
Sn _H	3.15	3.15	2.68	2.68
Sn _{N,planar}	4.90	5.00	4.71	4.82
Sn _{Ga,planar}	2.16	2.06	2.16	2.06
Sn _{N,buckling}	2.23	2.33	2.11	2.21
Sn _{Ga,buckling}	1.77	1.67	1.62	1.52

3.2. Single group-IV atom doping in monolayer GaN

We expanded current calculations to the doping of other group-IV atom X (X = C, Si, Sn) in monolayer GaN. Both C_{Ga,buckling} structures and Si_{Ga,buckling} structures are not stable and will transition into the NM planar doping configuration after structural relaxation. The C and Si atoms have smaller atomic radii than that of the Ga atom. Their valence electrons can effectively participate in the bonding with neighboring N atoms when they stay in the GaN plane. Meanwhile, all the valence electrons become nonlocalized bonding electrons, so no magnetic moment appears. Their buckling doping structure will weaken the C-N or Si-N bonding, so has higher energy than that of planar doping configuration. As a result, both of them can not introduce magnetism in monolayer GaN.

Similar to the Ge dopant, Sn atom prefers the buckling doping structure Sn_{Ga,buckling} with a magnetic moment of 1 μ_B per Sn atom [see figure A1(b)]. The corresponding E_f is lower in the N-rich growth conditions [see table 2]. Thus, the Sn atom is also suited for inducing magnetic properties into monolayer GaN. The Ge and Sn atoms have large atomic radii and feel the strain in the X_{Ga,planar} structure. Their buckling doping structures can effectively release the strain, thereby decreasing the total energy. The buckling structure offers a sp^3 -like bonding environment. A valence electron of Ge or Sn becomes an unpaired and localized electron which produces a magnetic moment of 1 μ_B .

The buckling height of the Sn atom in Sn_{Ga,buckling} is about 0.9 Å, larger than that of the Ge atom. Similarly, the spin density is mainly located on the Sn atom and its three nearest N atoms. The Sn dopant in Sn_{Ga,buckling} structure introduces two dispersionless impurity bands with different spins in the fundamental band gap of monolayer GaN [see figure A2(a)]. The splitting of the spin-up and spin-down bands causes Sn_{Ga,buckling} to be a semiconductor with a band gap of 0.58 eV. The PDOS in figure A2(b) shows that the magnetic moment is dominated by the s and p_z orbitals of the Sn atom as well as the p_z orbital of the neighboring N atoms. As shown in table 3, the magnetic moment of Sn dopant also prefers to be in-plane. The MAE is almost isotropic and is about -121.27 μeV per Sn atom, which is larger than that of Ge dopant due the stronger SOC

of Sn atom than Ge atom.

The potential barrier ΔE to be overcome by the Sn atom crossing the GaN plane was estimated to be about 0.54 eV by the NEB method [44], which is larger than that of Ge atoms. The Sn atoms are less likely to cross the GaN plane than the Ge atoms. The in-plane diffusion of the Sn atom proceeds with the same diffusion path as that of the Ge atom. The corresponding ΔE is estimated as about 0.62 eV [see figure 2(b)], smaller than that of the Ge atom.

Table 3. The MAE (μeV per dopant atom) with magnetization along the different directions.

	[100]	[010]	[001]	[110]	[111]
Ge	0	0	14.55	-0.02	4.92
Sn	0	-0.05	121.27	-0.08	40.99

3.3. Strain effect

Strain is an effective way to modulate the structural and magnetic properties of 2D materials [45, 46, 47, 48, 49]. We defined the strain as $\varepsilon = \frac{(a-a_0)}{a_0} \times 100\%$, where a and a_0 are the lattice constants of the strained and unstrained structures, respectively. Compressive strain decreases the lattice constants of the $\text{Ge}_{\text{Ga,buckling}}$ and $\text{Sn}_{\text{Ga,buckling}}$ structures, but increases the buckling height d [see figure 3(a)]. The tensile strain has the opposite effect. The stretching of the lattice increases the space of the Ga vacancy, so that the Ge or Sn dopant gradually falls into the GaN plane. The $\text{Ge}_{\text{Ga,buckling}}$ and $\text{Sn}_{\text{Ga,buckling}}$ structures transfer to in-plane substituted structures at a tensile strain of 2% and 4%, respectively. Meanwhile, the magnetic moments of Ge and Sn dopant disappear at the corresponding tensile strains [see figure 3(b)]. As long as d does not approach 0, the substituted doping structure always has a magnetic moment, indicating a potential application in strain-switched spintronic devices.

The effect of strain on the MAE of Ge and Sn dopant is shown in figure 3(c) and 3(d). MAE remains negative at strain from -5% to 5%. Compressive and tensile strain will decrease and increase the MAE, respectively. Thus, compressive strain helps to enhance the in-plane magnetic anisotropy of $\text{Ge}_{\text{Ga,buckling}}$ and $\text{Sn}_{\text{Ga,buckling}}$ structures. To understand the physics mechanism behind the strain modulation of MAE, we displayed the orbital-resolved MAE of $\text{Sn}_{\text{Ga,buckling}}$ in figure 4(a). Based on the second-order perturbation theory [50], the MAE can be represented by

$$\text{MAE} = \zeta^2 \sum_{o,\alpha,u,\beta} (2\delta_{\alpha\beta} - 1) \frac{|\langle o^\alpha | \hat{L}_z | u^\beta \rangle|^2 - |\langle o^\alpha | \hat{L}_x | u^\beta \rangle|^2}{E_u^\alpha - E_o^\beta}. \quad (2)$$

Here ζ is the SOC strength. The α, β represent spin-up (\uparrow) or spin-down (\downarrow) state. E_o and E_u represent the energy of occupied (o) and unoccupied (u) states, respectively. The

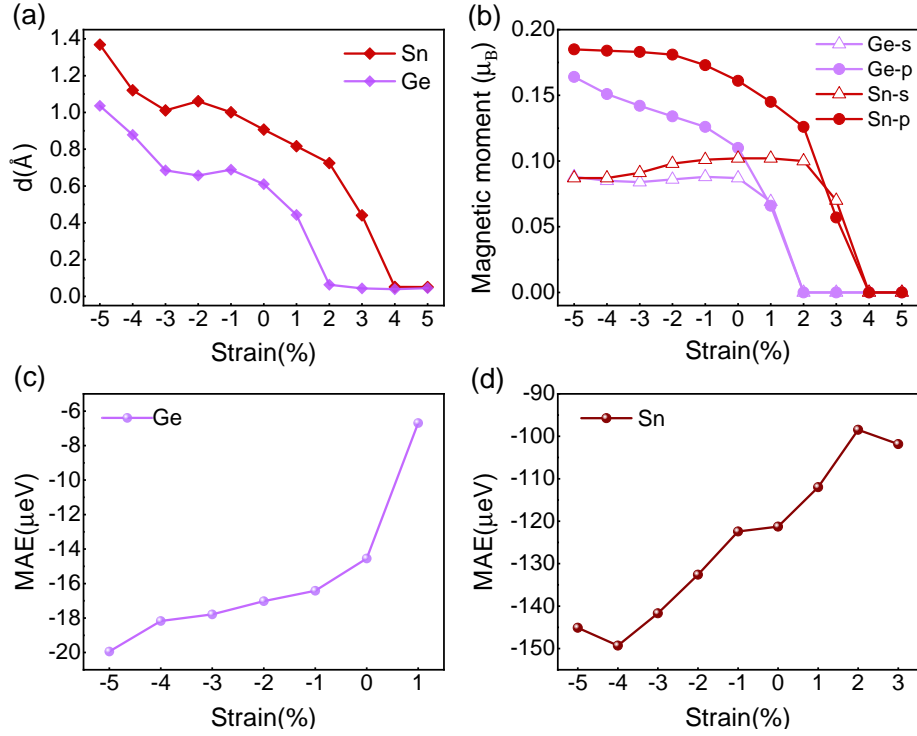


Figure 3. (a) The buckling height d and (b) orbital resolved magnetic moment as a function of strain. (c) and (d) are the MAE of $\text{Ge}_{\text{Ga,buckling}}$ and $\text{Sn}_{\text{Ga,buckling}}$ at different strains, respectively.

MAE was determined by the SOC matrix elements, the energy difference between the o and u states, and the density of o (u) states. The matrix element in the numerator of Eq. 2 is nonzero for $\langle m | \hat{L}_z | m \rangle$ and $\langle m | \hat{L}_x | m \pm 1 \rangle$, where m is the magnetic quantum number. Thus, the matrix element between p_z orbital is zero, though Sn- p_z orbital dominates the PDOS near the Fermi level [see figure A2(a)]. Combined the figure 4(a) and 4(b), the matrix element $\langle p_y^\dagger | \hat{L}_x | p_z^\dagger \rangle$ between the Sn- p_y state in the valence bands and the Sn- p_z state in the conduction bands make the main contribution to the negative MAE of $\text{Sn}_{\text{Ga,buckling}}$. Compressive strain enhances the σ -type bonding between the p_x and p_y orbital of Sn and neighboring N atoms. Since the energy of Sn- p orbital is higher than that of N- p orbital, the enhanced hybridization will further increase the energy of p_x and p_y orbital of Sn atom in the valence bands. As a result, the energy difference between the Sn- p_y state and Sn- p_z state decrease under compressive strain, as shown in see figure 4(b). The decrease of denominator $E_u - E_o$ of equation 2 leads to the decrease of the MAE of $\text{Sn}_{\text{Ga,buckling}}$ under compressive strain [see figure 3(d)]. The strain modulation of MAE of $\text{Ge}_{\text{Ga,buckling}}$ can be explained by similar analysis. Generally, $\text{Sn}_{\text{Ga,buckling}}$ has a larger SOC effect and a larger absolute value of MAE than that of $\text{Ge}_{\text{Ga,buckling}}$. Meanwhile, the magnetic moment of Sn dopant can sustain under a larger range of external strain than the Ge dopant [see figure 4(a)].

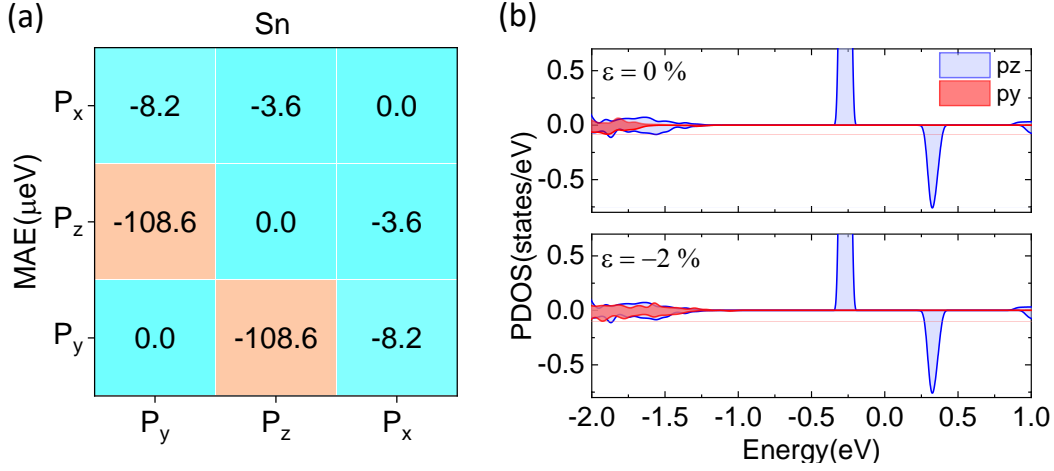


Figure 4. (a) orbital-resolved MAE of $\text{Sn}_{\text{Ga,buckling}}$ at strain of $\varepsilon = 0\%$. (b) The contribution of Sn- p_y and p_z orbital to the PDOS of $\text{Sn}_{\text{Ga,buckling}}$ p orbitals at a strain of 0% and -2%.

3.4. Magnetic coupling between group-IV dopant in monolayer GaN

To study the magnetic coupling between the group-IV dopants at high doping concentration, we substituted two Ga atoms with Ge or Sn atoms at different distances in a $10 \times 10 \times 1$ supercell of monolayer GaN [see figure 5(a)]. Meanwhile, we considered two doped atoms on the same or different sides of monolayer GaN [see figure 5(b)]. The possible magnetic coupling between two dopants includes ferromagnetic (FM), NM, and antiferromagnetic (AFM) coupling.

As shown in the figure 5(c, d), the doping configuration with the lowest energy is that two doped Ge or Sn atoms are located at opposite sides of monolayer GaN with the nearest distance. The corresponding doped configuration was labeled as (0, 1) which represent that a Ge atom is at the 0 site and the other one is located at the 1 site, as shown in figure 5(a). Meanwhile, we found that both FM and AFM states of the configuration (0, 1) were converted to the NM state. Therefore, when the distance between the group-IV dopants is too small, the aggregation phenomenon will occur and the magnetic moments of group-IV atoms disappear. However, we have found that the Ge and Sn atom have a large diffusion barrier ΔE vertical to the GaN plane. Especially, the ΔE of the Sn atom reaches 0.54 eV. Thus, if we grew monolayer GaN on a suitable substrate and doped it with Ge or Sn atoms from one side of monolayer GaN, most of dopants might stay on the same side of monolayer GaN. For Ge or Sn atoms on the same side of monolayer GaN, the (0, 2) configuration in the AFM state has the lowest energy, as shown in figure 5(c, d). The dopant-dopant distance is about 5.7 Å. As the distance between two doped atoms increases, the magnetic coupling between them gradually decreases. The difference between the energy of FM and AFM state becomes small at a large distance.

Figure 6(a) displays the spin distribution of the configuration (0, 2) in the AFM

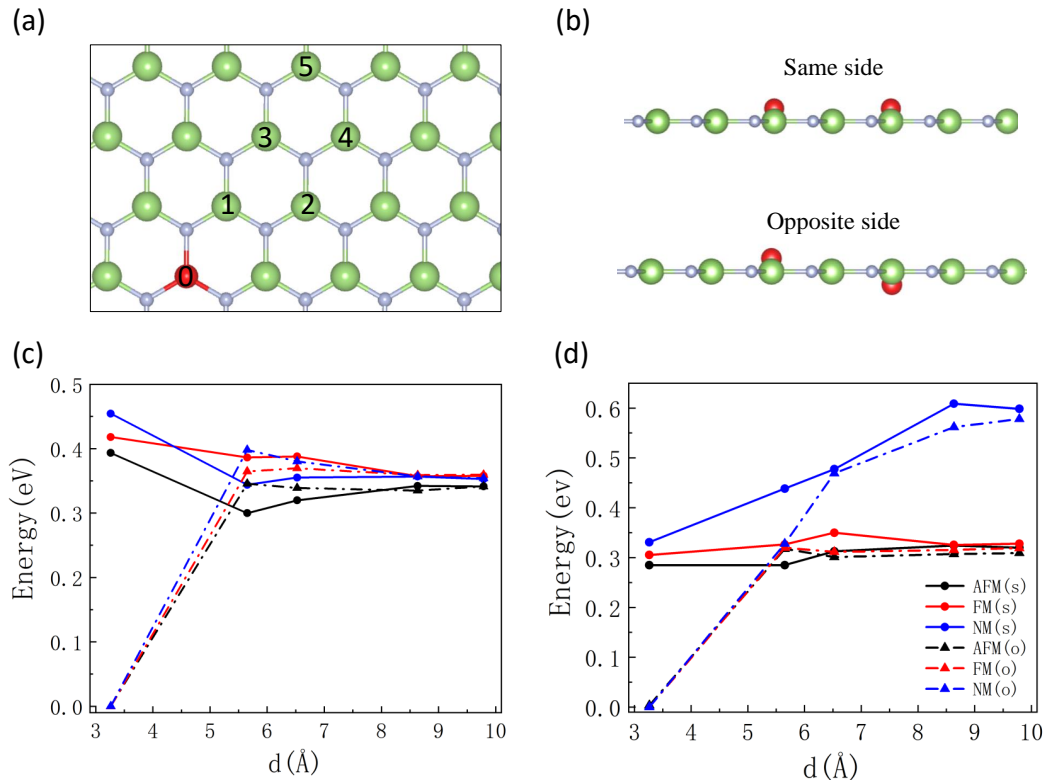


Figure 5. (a) The doping position of double Ge atoms in monolayer GaN. One is located at site 0, the other one is located at 1 ~ 5 site. (b) The Schematic diagram of two doped Ge atom on the same (S) and opposite (O) side of monolayer GaN. The total energy as a function of distance between the doped (c) Ge atom and (d) Sn atoms. The energy of doped monolayer GaN with the nearest dopant distance was set to 0.

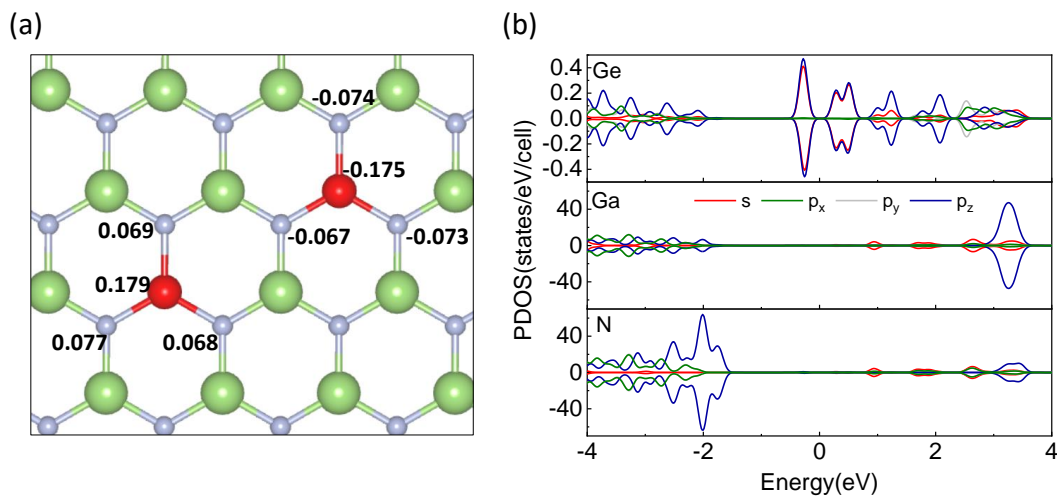


Figure 6. (a) The distribution of magnetic moment of monolayer GaN doped with double Ge atoms in the antiferromagnetic state. (b) The corresponding PDOS of doped configuration in (a).

state. It can be seen that the doped Ge atoms and their nearest N atoms provide the largest contribution to the magnetic moments. The direction of magnetic moments is the same for Ge and its neighboring N atoms, but is different for two doped Ge atoms. The corresponding PDOS in figure 6(b) shows a symmetric DOS in the spin-up and spin-down channels. Through the checking of the PDOS of monolayer GaN with two doped Ge atoms on the same side, we found that all the double doped GaN exhibited AFM semiconducting properties [see figure 6(b)]. The s and p_z orbitals of the Ge atoms dominate the PDOS at the Fermi level. The representative spin distribution and PDOS of the AFM state of monolayer GaN with two doped Sn atoms is shown in figure A3, which also exhibits similar AFM semiconducting properties.

We noticed that if one fully substituted Ga atoms by Ge or Sn atoms, one can obtain monolayer GeN and SnN which are FM semiconductors with large band gap and high Curie temperatures [13, 52]. Thus, there should be an AFM-to-FM magnetic transition in group-IV doped monolayer GaN as the doping concentration increases, which can be explained by the enhanced exchange splitting and delocalized impurity states of group-IV dopants [13].

3.5. The influence of intrinsic vacancy on the group-IV-doped monolayer GaN

At last, we considered the effect of intrinsic vacancies on the magnetic properties of group-IV-doped monolayer GaN. We first created a Ga vacancy (V_{Ga}) or N vacancy (V_{N}) in a $6 \times 6 \times 1$ GaN supercell and calculated its magnetic state. We found that the size of the \mathbf{k} -grid mesh was crucial to appropriately predict the ground magnetic state of intrinsic vacancies of monolayer GaN. For example, one might predict V_{N} to be a NM state with a coarse \mathbf{k} -grid mesh. However, V_{N} should be in the magnetic state with a magnetic moment of $1 \mu_B$ using a dense \mathbf{k} -grid mesh. That can explain the contradiction in previous works [31, 30]. Next, we substituted one Ga atom in the $6 \times 6 \times 1$ GaN supercell, and two Ga atoms in a $10 \times 10 \times 1$ supercell of by group-IV atom X ($X = \text{Ge}, \text{Sn}$). The group-IV dopants are in the stable $\text{Ge}_{\text{Ga,buckling}}$ or $\text{Sn}_{\text{Ga,buckling}}$ configuration. For monolayer GaN with two doped Ge or Sn atom, we choose the configuration (0, 2) as the representative configuration [see figure 5(a)]. Meanwhile, two Ge or Sn atoms are in the AFM configuration and locate on the same side of monolayer GaN. Then we created a Ga or N vacancy (V_{Ga}) at different distance d between the vacancy and the dopants in the supercell of monolayer GaN.

3.5.1. N vacancy For the case of N vacancy, we found that group-IV-doped monolayer GaN containing a N vacancy always exhibit the NM state. Thus, N vacancy is not desirable for magnetic properties of group-IV-doped monolayer GaN. According to previous content, the N-rich growth conditions are more favorable for not only substituting of the Ga atoms by group-IV atoms but also preventing the forming of N vacancies in monolayer GaN. Cui et al. had proposed that the disproportionation of NO can be used to repair the N-vacancy of monolayer InN [53]. Similar methods can be

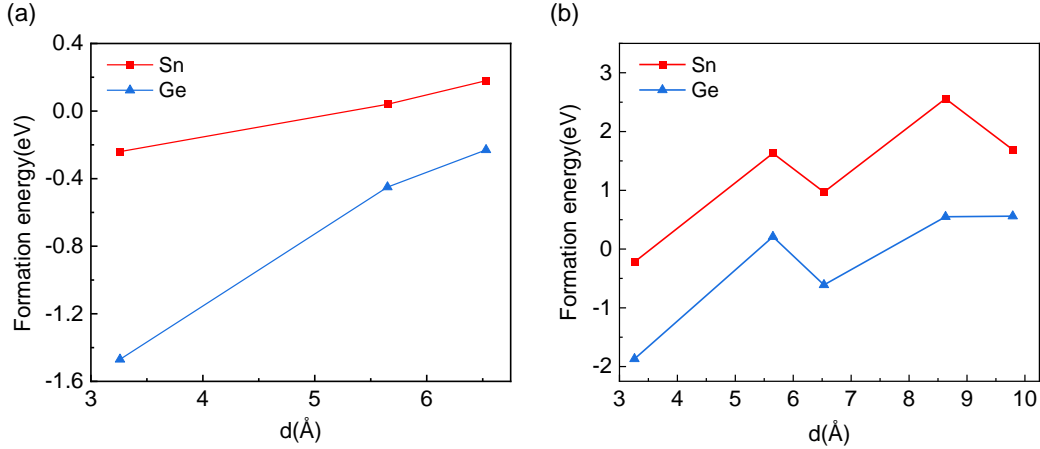


Figure 7. The formation energy of group-IV-doped monolayer GaN with a Ga vacancy (a) $V_{\text{Ga}} + X$ and $V_{\text{Ga}} + 2X$ as a function of distance between the dopant and Ga vacancy in the N-rich growth conditions. X present the group-VI dopant Ge and Sn.

applied in monolayer GaN to decrease the concentration of N vacancies in the future.

3.5.2. Ga vacancy We labeled group-IV-doped monolayer GaN with a Ga vacancy and one or two dopants as $V_{\text{Ga}} + X$ or $V_{\text{Ga}} + 2X$ configurations, respectively. As shown in figure 7 (a, b), the relevant E_f of $V_{\text{Ga}} + X$ or $V_{\text{Ga}} + 2X$ are even negative for small d . The E_f in general increases as with the d increasing. That indicated that the V_{Ga} tends to get close to Ge or Sn dopants to form complex structures.

The representative distribution of spin density and band structures for $V_{\text{Ga}} + \text{Sn}$ at different d are displayed in figure 8 (a, b). Moreover, the band gap is insensitive to d . A similar situation was also founded in $V_{\text{Ga}} + \text{Ge}$ structures. The band gap of $V_{\text{Ga}} + \text{Ge}$ or $V_{\text{Ga}} + \text{Sn}$ at different d is about 1.00 eV and 0.60 eV, respectively. Though $V_{\text{Ga}} + \text{Sn}$ also exhibit the spin-polarized band structure, the spin density is mainly distributed on the N atoms near the Ga vacancy. The spin density around the group-IV dopant is negligible. The similar situation happens in $V_{\text{Ga}} + 2X$ configurations. Through the examination of the lattice structure of $V_{\text{Ga}} + X$ or $V_{\text{Ga}} + 2X$ configurations, we found that the group-IV dopant returned to the GaN plane in the presence of V vacancy. That means that all the valence electrons of group-IV dopants become bonding electrons and can not exhibit magnetic moments.

Each Ga vacancy in monolayer GaN leaves three unpaired electrons on the three neighboring N atoms around the Ga vacancy, leading to the magnetic moment of $3 \mu_B$ [31]. When another Ga atom was replaced by Ge or Sn atom, an extra electron was brought in monolayer GaN. However, at this moment, we found that the extra electron could not keep around the dopant as the unpaired electron, but transfer to the N atoms near the Ga vacancy to fill a hole. As a result, the magnetic moment of $V_{\text{Ga}} + \text{Ge}$ or $V_{\text{Ga}} + \text{Sn}$ is only $2 \mu_B$. The transferring of charge was found even in the $V_{\text{Ga}} + X$

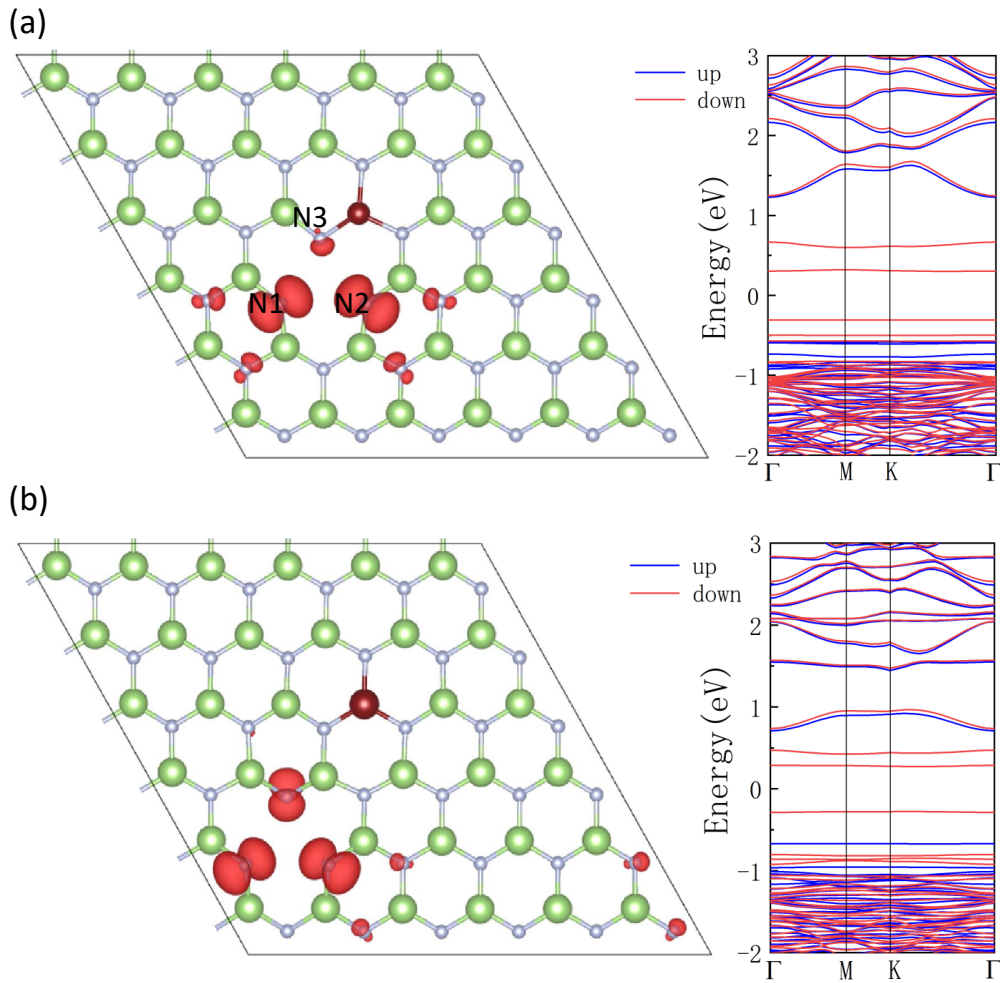


Figure 8. Spin density and band structure of $V_{\text{Ga}} - \text{Sn}$ with (a) small and (b) large distance between dopant and vacancy. Positive and negative spin density are labeled as red and yellow, respectively. The spin-equivalent surface is $0.0035 \text{ eV}/\text{\AA}^3$.

configurations with a large d . Similarly, we found that the magnetic moments of most $V_{\text{Ga}} + 2\text{X}$ configurations are $1 \mu_B$, due to that two extra electrons transfer from two group-VI dopants to the N atoms near the Ga vacancy. At the moment, Ge or Sn atoms were only used to tune the magnetic moment of Ga vacancy by changing the hole number, rather than induce magnetic moment. Therefore, the Ga vacancy will also remove the unpaired electron on the Ge or Sn dopant, which is not desirable for the magnetic properties of group-IV doped monolayer GaN.

How to avoid such situation? Beginning with monolayer GaN with a Ga vacancy (V_{Ga}), we compared the formation energy E_f of two process. One is that Ge or Sn atom directly fulfills the Ga vacancy, and the other one is that Ge or Sn atom substitutes another Ga atom in the monolayer GaN. The E_f of former process is much smaller than the later one. Thus, the doping group-IV atoms are more inclined to fill the intrinsic Ga vacancies directly. If one supplied enough concentration of Ge or Sn dopants into

monolayer GaN in the N-rich growth conditions, most Ge or Sn atoms will mainly form the $\text{Ge}_{\text{Ga,buckling}}$ or $\text{Sn}_{\text{Ga,buckling}}$ configurations. Meanwhile, the forming of intrinsic Ga and N vacancies can be effectively suppressed, which helps to realize the introduction of magnetic properties into monolayer GaN.

4. Conclusion

In conclusion, using first-principle calculations, we predicted that both Ge and Sn atoms are likely to replace the Ga atoms of monolayer GaN, forming a buckling structure with a buckling height of 0.6 Å and 0.9 Å respectively. The diffusion barriers of the Ge atom along the direction vertical and parallel to the monolayer GaN are 0.12 eV and 0.82 eV, respectively. The corresponding diffusion barriers for the Sn atom are 0.54 eV and 0.62 eV, respectively. Single Ge- and Sn-doped monolayer GaN exhibit as a semiconductor with a band gap of 0.40 and 0.58 eV, respectively. Both Ge and Sn dopants can exhibit a magnetic moment of $1 \mu_B$ which prefers lying in the xy -plane. The in-plane MAE is $-14.55 \mu\text{eV}$ and $-121.27 \mu\text{eV}$ for Ge and Sn dopant, respectively. Compressive strain enhances the magnetic moment and MAE of the group-VI dopant, while a large tensile strain will destroy the magnetic moment of dopant. Sn is better than Ge for the introduction of magnetic properties into monolayer GaN due to larger SOC, MAE, vertical diffusion barrier, and strain range to maintain the magnetic moment. As the doping concentration increases, the large vertical diffusion barrier to the monolayer GaN can be used to make both Ge and Sn atoms stay on the same side of monolayer GaN with an antiferromagnetic coupling between them. Both N vacancies and Ga vacancies will remove the magnetic moment of Ge or Sn dopants. The plentiful supply of Ge or Sn dopants and the N-rich growth conditions help to realize the introduction of the magnetic properties into monolayer GaN for the spintronic applications.

5. Acknowledgments

This work was supported by National Natural Science Foundation of China (No. 11904313 and 11904312), the Scientific Research Foundation of the Higher Education of Hebei Province, China (No. BJ2020015), the Natural Science Foundation of Hebei Province (No. A2020203027), the Doctor Foundation Project of Yanshan University (No. BL19008). Innovation Capability Improvement Project of Hebei province (No. 22567605H). The numerical calculations in this paper have been done on the supercomputing system in the High Performance Computing Center of Yanshan University

Appendix A.

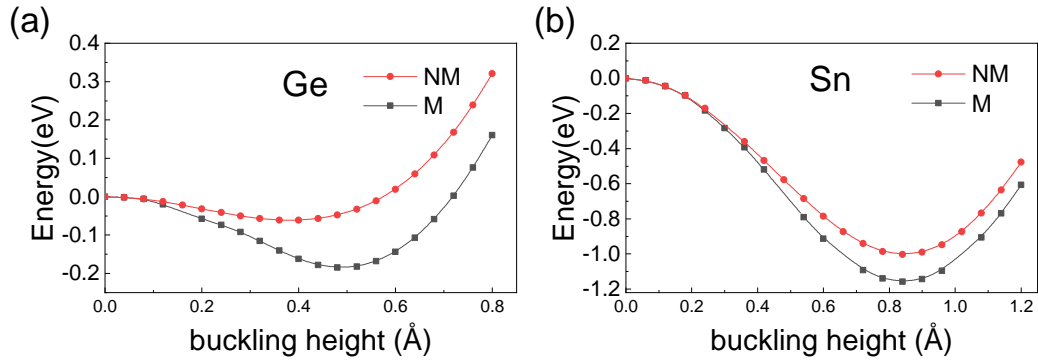


Figure A1. The energy of (a) Ge_{Ga,buckling} and (b) Sn_{Ga,buckling} as a function of buckling height in non-magnetic (NM) and magnetic (M) state. The energy of planar doping structure was set to be zero. Here, the energies of buckling structure were calculated without structural relaxation of atomic position.

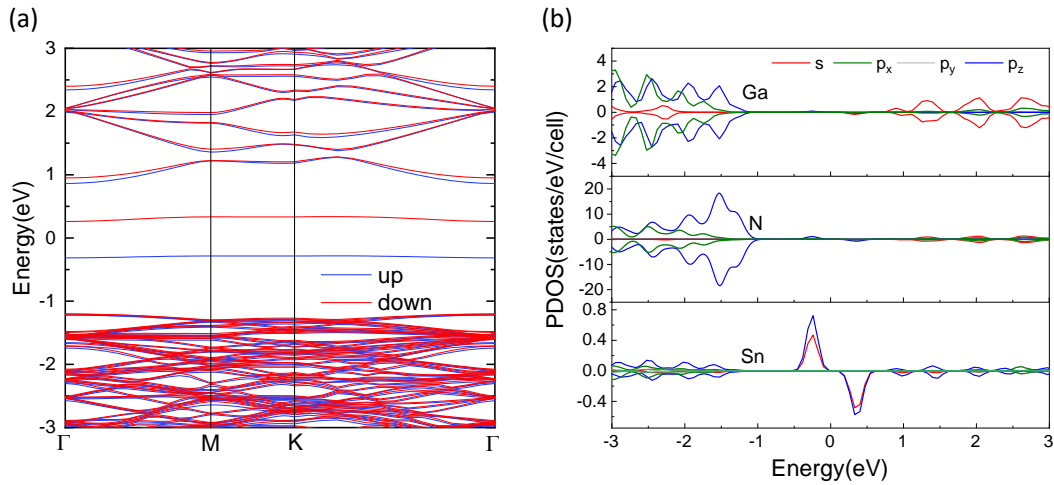


Figure A2. (a) Energy bands and (b) PDOS of Sn_{Ga,buckling} configuration.

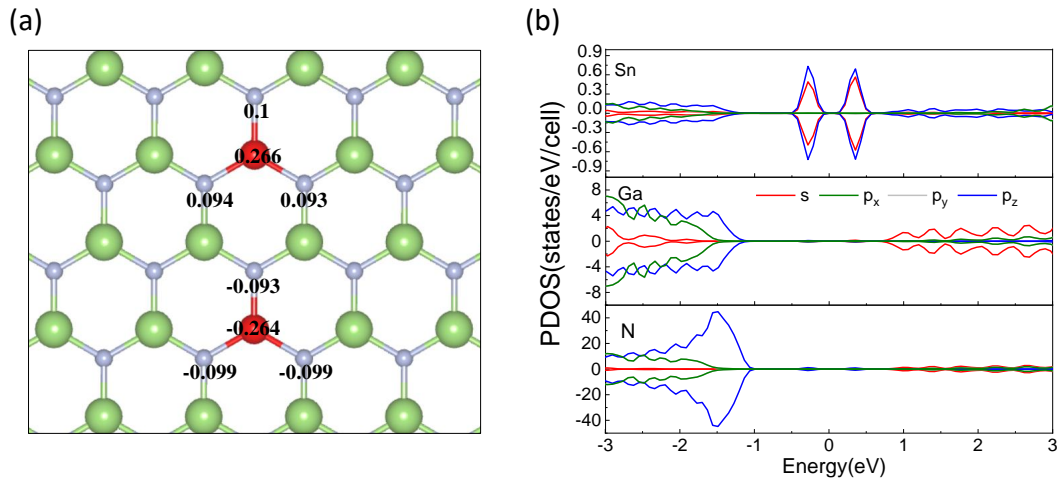


Figure A3. (a) The main magnetic moment distribution of monolayer GaN doped with double Sn atoms in the same side of monolayer GaN. (b) The corresponding PDOS of configuration as shown in (a).

- [1] T. Jungwirth, Jairo Sinova, J. Mašek, J. Kučera, and A. H. MacDonald. Theory of ferromagnetic (III,Mn)V semiconductors. *Rev. Mod. Phys.*, 78:809–864, Aug 2006.
- [2] T Dietl and H Ohno. Ferromagnetism in III–V and II–VI semiconductor structures. *Physica E*, 9(1):185–193, 2001.
- [3] X. Y. Cui, J. E. Medvedeva, B. Delley, A. J. Freeman, N. Newman, and C. Stampfl. Role of embedded clustering in dilute magnetic semiconductors: Cr Doped GaN. *Phys. Rev. Lett.*, 95:256404, Dec 2005.
- [4] Chenwei Zhang, Penghui Yin, Wenhuan Lu, Victor Galievsky, and Pavle V. Radovanovic. On the origin of d_0 magnetism in transparent metal oxide nanocrystals. *J. Phys. Chem. C*, 125(50):27714–27722, 2021.
- [5] Brahmananda Chakraborty and Lavanya M. Ramaniah. Exploring d_0 magnetism in doped SnO_2 —a first principles DFT study. *J. Magn. Magn. Mater.*, 385:207–216, 2015.
- [6] J. M. D. Coey. Magnetism in d_0 oxides. *Nat. Mater.*, 18(7):652–656, 2019.
- [7] Bevin Huang, Genevieve Clark, Efrén Navarro-Moratalla, Dahlia R. Klein, Ran Cheng, Kyle L. Seyler, Ding Zhong, Emma Schmidgall, Michael A. McGuire, David H. Cobden, Wang Yao, Di Xiao, Pablo Jarillo-Herrero, and Xiaodong Xu. Layer-dependent ferromagnetism in a van der waals crystal down to the monolayer limit. *Nature*, 546(7657):270–273, 2017.
- [8] Cheng Gong, Lin Li, Zhenglu Li, Huiwen Ji, Alex Stern, Yang Xia, Ting Cao, Wei Bao, Chenzhe Wang, Yuan Wang, Z. Q. Qiu, R. J. Cava, Steven G. Louie, Jing Xia, and Xiang Zhang. Discovery of intrinsic ferromagnetism in two-dimensional van der waals crystals. *Nature*, 546(7657):265–269, 2017.
- [9] Weiwei Ju, Tongwei Li, Zhiwei Hou, Hui Wang, Hongling Cui, and Xiaohong Li. Exotic d_0 magnetism in partial hydrogenated silicene. *Appl. Phys. Lett.*, 108(21):212403, 2016.
- [10] Zijian Gao, Weiwei Ju, Tongwei Li, Qingxiao Zhou, Donghui Wang, Yi Zhang, and Haisheng Li. Tunable magnetism in defective MoS_2 monolayer with nonmetal atoms adsorption. *Superlattices Microstruct.*, 130:346–353, 2019.
- [11] Yujie Bai, Kaiming Deng, and Erjun Kan. Electronic and magnetic properties of an AlN monolayer doped with first-row elements: a first-principles study. *RSC Adv.*, 5:18352–18358, 2015.
- [12] Ruilin Han, Xiaoyang Chen, and Yu Yan. Magnetic properties of AlN monolayer doped with group 1A or 2A nonmagnetic element: First-principles study. *Chin. Phys. B*, 26(9):097503, aug 2017.

- [13] Wenhui Wan, Na Kang, Yanfeng Ge, and Yong Liu. The theoretical study of unexpected magnetism in 2D Si-Doped AlN. *Front. Phys.*, 10:843352, 2022.
- [14] Wen-Zhi Xiao, Gang Xiao, Qing-Yan Rong, and Ling-Ling Wang. Electronic and magnetic properties of SnS₂ monolayer doped with non-magnetic elements. *Physica E*, 99:182–188, 2018.
- [15] Kalyan Adhikary and Subhadra Chaudhuri. Gallium nitride: Synthesis and characterization. *Trans. Indian Ceram. Soc.*, 66(1):1–16, 2007.
- [16] Haneen D. Jabbar, Makram A. Fakhri, and Mohammed Jalal AbdulRazzaq. Gallium nitride –based photodiode: A review. *Mater. Today: Proc.*, 42:2829–2834, 2021.
- [17] Wesley J. de Paula, Pedro L. Tavares, Denis De C. Pereira, Gabriel M. Tavares, Filipe L. Silva, Pedro S. Almeida, and Henrique A. C. Braga. A review on gallium nitride switching power devices and applications. In *2017 Brazilian Power Electronics Conference (COBEP)*, pages 1–7, 2017.
- [18] Xing Xiang Ruan, Cansheng Huang, Fuchun Zhang, Hui Fang, and Weihua Zhang. First-principles study on electromagnetic properties of Mn-doped GaN. *Ferroelectrics*, 547:104 – 97, 2019.
- [19] P.R. Hageman, W.J. Schaff, Jacek Janinski, and Zuzanna Liliental-Weber. n-type doping of wurtzite GaN with germanium grown with plasma-assisted molecular beam epitaxy. *J. Cryst. Growth*, 267(1):123–128, 2004.
- [20] S. Fritze, A. Dadgar, H. Witte, M. Bügler, A. Rohrbeck, J. Bläsing, A. Hoffmann, and A. Krost. High Si and Ge n-type doping of GaN doping - Limits and impact on stress. *Appl. Phys. Lett.*, 100(12):122104, 2012.
- [21] Zakaria Y. Al Balushi, Ke Wang, Ram Krishna Ghosh, Rafael A. Vilá, Sarah M. Eichfeld, Joshua D. Caldwell, Xiaoye Qin, Yu-Chuan Lin, Paul A. DeSario, Greg Stone, Shruti Subramanian, Dennis F. Paul, Robert M. Wallace, Suman Datta, Joan M. Redwing, and Joshua A. Robinson. Two-dimensional gallium nitride realized via graphene encapsulation. *Nat. Mater.*, 15(11):1166–1171, 2016.
- [22] Nikhil A. Koratkar. Two-dimensional gallium nitride. *Nat. Mater.*, 15(11):1153–1154, 2016.
- [23] Jiabin Li and Hongxia Liu. Magnetism investigation of GaN monolayer doped with group VIII B transition metals. *J. Mater. Sci.*, 53(23):15986–15994, 2018.
- [24] Gang Xiao, Ling-Ling Wang, Qing-Yan Rong, Hai-Qing Xu, and Wen-Zhi Xiao. A comparative study on magnetic properties of Mo doped AlN, GaN and InN monolayers from first-principles. *Phys. B*, 524:47–52, 2017.
- [25] Fayyaz Hussain, Y. Q. Cai, M. Junaid Iqbal Khan, Muhammad Imran, Muhammad Rashid, Hafeez Ullah, Ejaz Ahmad, Farhana Kousar, and S. A. Ahmad. Enhanced ferromagnetic properties of Cu doped two-dimensional GaN monolayer. *Int. J. Mod. Phys. C*, 26(01):1550009, 2015.
- [26] Basanta Roul, Mohana K. Rajpalke, Thirumaleshwara N. Bhat, Mahesh Kumar, A. T. Kalghatgi, S. B. Krupanidhi, Nitesh Kumar, and A. Sundaresan. Experimental evidence of Ga-vacancy induced room temperature ferromagnetic behavior in GaN films. *Appl. Phys. Lett.*, 99(16):162512, 2011.
- [27] Qian Zhao, Zhihua Xiong, Zhenzhen Qin, Lanli Chen, Ning Wu, and Xingxing Li. Tuning magnetism of monolayer GaN by vacancy and nonmagnetic chemical doping. *J. Phys. Chem. Solids*, 91:1–6, 2016.
- [28] Vo Van On, J. Guerrero-Sanchez, R. Ponce-Pérez, and D.M. Hoat. Study of vacancy, voids, atom adsorption and domain substitution in hexagonal gallium nitride monolayer. *Surf. Interfaces*, 30:101898, 2022.
- [29] M. G. Ganchenkova and R. M. Nieminen. Nitrogen vacancies as major point defects in gallium nitride. *Phys. Rev. Lett.*, 96:196402, May 2006.
- [30] Roberto González, William López-Pérez, Álvaro González-García, María G. Moreno-Armenta, and Rafael González-Hernández. Vacancy charged defects in two-dimensional GaN. *Appl. Surf. Sci.*, 433:1049–1055, 2018.
- [31] Han Gao, Han Ye, Zhongyuan Yu, Yunzhen Zhang, Yumin Liu, and Yinfeng Li. Point defects and composition in hexagonal group-III nitride monolayers: A first-principles calculation.

- Superlattices Microstruct.*, 112:136–142, 2017.
- [32] Yuewen Mu. Chemical functionalization of GaN monolayer by adatom adsorption. *J. Phys. Chem. C*, 119(36):20911–20916, 2015.
- [33] Wencheng Tang, Minglei Sun, Jin Yu, and Jyh-Pin Chou. Magnetism in non-metal atoms adsorbed graphene-like gallium nitride monolayers. *Appl. Surf. Sci.*, 427:609–612, 2018.
- [34] Yelda Kadioglu, Fatih Ersan, Deniz Kecik, Olcay Üzengi Aktürk, Ethem Aktürk, and Salim Ciraci. Chemical and substitutional doping, and anti-site and vacancy formation in monolayer AlN and GaN. *Phys. Chem. Chem. Phys.*, 20:16077–16091, 2018.
- [35] Naresh Alaal and Iman S. Roqan. Tuning the electronic properties of hexagonal two-dimensional GaN monolayers via doping for enhanced optoelectronic applications. *ACS Appl. Nano Mater.*, 2(1):202–213, 2019.
- [36] Sandeep Yadav, B.K. Agrawal, and P.S. Yadav. Non-magnetic adsorbent functionalized magnetism and spin filtering in a two-dimensional GaN monolayer. *J. Phys. Chem. Solids*, 167:110731, 2022.
- [37] Sanjeev K. Gupta, Haiying He, Douglas Banyai, Mingsu Si, Ravindra Pandey, and Shashi P. Karna. Effect of Si doping on the electronic properties of BN monolayer. *Nanoscale*, 6:5526–5531, 2014.
- [38] G. Kresse and J. Furthmüller. Efficient iterative schemes for ab initio total-energy calculations using a plane-wave basis set. *Phys. Rev. B*, 54:11169–11186, Oct 1996.
- [39] G. Kresse and D. Joubert. From ultrasoft pseudopotentials to the projector augmented-wave method. *Phys. Rev. B*, 59:1758–1775, Jan 1999.
- [40] John P Perdew, Kieron Burke, and Matthias Ernzerhof. Generalized gradient approximation made simple. *Phys. Rev. Lett.*, 77(18):3865, 1996.
- [41] Hendrik J Monkhorst and James D Pack. Special points for Brillouin-zone integrations. *Phys. Rev. B*, 13(12):5188, 1976.
- [42] X. Y. Cui, B. Delley, and C. Stampfl. Band gap engineering of wurtzite and zinc-blende GaN/AlN superlattices from first principles. *J. Appl. Phys.*, 108(10):103701, 2010.
- [43] Heinz Schulz and K.H. Thiemann. Crystal structure refinement of AlN and GaN. *Solid State Commun.*, 23(11):815–819, 1977.
- [44] Gregory Mills, Hannes Jónsson, and Gregory K. Schenter. Reversible work transition state theory: application to dissociative adsorption of hydrogen. *Surf. Sci.*, 324(2):305–337, 1995.
- [45] Xiaotian Fang, Baozeng Zhou, Xiaocha Wang, and Wenbo Mi. High curie temperature and large perpendicular magnetic anisotropy in two-dimensional half metallic osi3 monolayer with quantum anomalous hall effect. *Mater. Today Phys.*, 28:100847, 2022.
- [46] Yuwan Wang, Xicheng Zhang, Zhihao Gao, Tengfei Cao, Junqin Shi, and Xiaoli Fan. Ferromagnetic gdx (x = cl, br) monolayers with large perpendicular magnetic anisotropy and high curie temperature. *J. Phys. Chem. C*, 127(9):4643–4650, 2023.
- [47] Shengmei Qi, Jiawei Jiang, Xiaocha Wang, and Wenbo Mi. Valley polarization, magnetic anisotropy and dzyaloshinskii-moriya interaction of two-dimensional graphene/janus 2h-vsex (x = s, te) heterostructures. *Carbon*, 174:540–555, 2021.
- [48] Shiming Yan, Wen Qiao, Deyou Jin, Xiaoyong Xu, Wenbo Mi, and Dunhui Wang. Role of exchange splitting and ligand-field splitting in tuning the magnetic anisotropy of an individual iridium atom on Tas₂ substrate. *Phys. Rev. B*, 103:224432, Jun 2021.
- [49] Fang Zhang, Wenbo Mi, and Xiaocha Wang. Spin-dependent electronic structure and magnetic anisotropy of 2d ferromagnetic janus cr2i3x3 (x = br, cl) monolayers. *Adv. Electron. Mater.*, 6(1):1900778, 2020.
- [50] Ding-sheng Wang, Ruqian Wu, and A. J. Freeman. First-principles theory of surface magnetocrystalline anisotropy and the diatomic-pair model. *Phys. Rev. B*, 47:14932–14947, Jun 1993.
- [51] Gerrit van der Laan. Microscopic origin of magnetocrystalline anisotropy in transition metal thin films. *J. Phys.: Condens. Matter*, 10(14):3239, apr 1998.
- [52] Nikolay V. Tkachenko, Bingyi Song, Dmitriy Steglenko, Ruslan M. Minyaev, Li-Ming Yang, and Alexander I. Boldyrev. Computational prediction of the low-temperature ferromagnetic

- semiconducting 2D SiN monolayer. *Phys Status Solidi B*, 257(3):1900619, 2020.
- [53] Hao Cui, Dachang Chen, Chao Yan, Ying Zhang, and Xiaoxing Zhang. Repairing the N-vacancy in an InN monolayer using NO molecules: a first-principles study. *Nanoscale Adv.*, 1:2003–2008, 2019.